SOHO: Orthogonal and Symmetric Haar Wavelets on the Sphere

CHRISTIAN LESSIG and EUGENE FIUME
University of Toronto

In this work we propose the SOHO wavelet basis. To our knowledge this is the first spherical Haar wavelet basis that is both orthogonal and symmetric, making it particularly well suited for the approximation and processing of all-frequency signals on the sphere. The key to the derivation of the basis is a novel spherical subdivision scheme that defines a partition acting as domain of the basis functions. The construction of the SOHO wavelets refutes earlier claims doubting the existence of such a basis. Experimental results for the representation of spherical signals verify that the superior theoretical properties of the SOHO wavelet basis are also relevant in practice.

Categories and Subject Descriptors: I.3.0 [**Computing Methodologies**]: Computer Graphics—*General*; G.1.0 [**Numerical Analysis**]: General—*Numerical Algorithms*; G.1.2 [**Numerical Analysis**]: Approximation—*Nonlinear Approximation*

General Terms: Theory, Measurement

Additional Key Words and Phrases: wavelet transform, spherical signals

1. INTRODUCTION

Many signals are naturally parametrized over the sphere $\mathbb{S}^2$. Examples from computer graphics include bidirectional reflectance distribution functions (BRDFs), radiance, and visibility. Spherically parametrized signals can also be found in many other fields, including astronomy, physics, climate modeling, and medical imaging. An efficient and distortion free representation of spherical signals is therefore of importance for many applications. Of particular interest are the ability to approximate a wide range of signals accurately with a small number of basis function coefficients, and the possibility of obtaining computationally efficient algorithms to process a signal in its basis representation.

A variety of representations for spherical signals has been proposed in the literature. Spherical Harmonics (SH) have been particularly popular for the representation of low-frequency signals. The global support of the basis functions, however, makes

Authors' address: {lessig | elf}@dgp.toronto.edu, C. Lessig, E. Fiume, Dynamic Graphics Project, Department of Computer Science, University of Toronto, 40 St. George Street, M5S 2E4 Toronto, ON, Canada

the SH basis inefficient for representing high-frequency data, and for processing signals in the basis representation. Spherical Radial Basis Functions (SRBF) are localized in both space and frequency and are thus efficient for the representation of all-frequency signals. Unfortunately, projecting a signal into an SRBF basis is prohibitively expensive, and efficiently processing a signal is difficult due to the unstructured nature of the bases. Wavelets in contrast are hierarchically structured; together with the localization in space and frequency leading to fast algorithms both for basis projection and for processing signals in the basis representation. Wavelet bases are also designed to represent dissimilarities in a signal, making them well suited for compact representation and approximation of typical signals.

In the past, wavelets parametrized over planar domains have often been used to represent spherical signals. Such representations suffer, however, from parametrization artifacts which are unavoidable when the sphere is mapped onto a planar domain. Spherical wavelets are free of distortion but the representations proposed in the literature are limited in their ability to efficiently approximate and process all-frequency signals. We argue that the following three properties are important for an efficient representation.

Orthogonality. An orthogonal basis has a variety of theoretical and practical advantages. Most notably, the optimal approximation in the ℓ_2 norm can be found efficiently. In many cases orthogonality also leads to more efficient algorithms, for example for computing product integrals, and establishing properties of a representation is often easier for orthogonal bases.

(Very) Compact Support. The costs of performing wavelet transforms and of processing a signal in its basis representation depend heavily on the support size of a basis. Haar-like bases have minimal support and computations in this representation are thus very efficient. In the literature it has often been argued that Haar-like bases are well suited only for the representation of piecewise constant functions. Both theoretical and practical results have shown, however, that they also efficiently represent functions of bounded variation, that is all-frequency signals as found in many applications.

Symmetry. Symmetry guarantees an orientation-free representation of features in the basis, preventing distortion when a signal is approximated in its basis representation. The high sensitivity of the human visual system to asymmetric artifacts makes this particularly important for the visual quality of approximated signals.

We conclude that an orthogonal and symmetric spherical Haar wavelet basis is particularly well suited for the efficient approximation and processing of all-frequency signals on the sphere. However, none of the bases proposed in the literature satisfy all of the above properties. We therefore developed the *SOHO wavelet basis* that to our knowledge is the first spherical Haar wavelet basis that is both orthogonal and symmetric. The key to the derivation of the basis is a novel subdivision scheme of the sphere that defines a partition acting as the domain of the basis functions. The derivation of the SOHO wavelets refutes earlier claims doubting the existence of such a basis (e.g., [Bonneau 1999]).

The practical relevance of the superior theoretical properties of the SOHO wavelet basis has been validated experimentally. Results for the representation of different spherical signals show that the SOHO wavelet basis provides competitive or lower error rates than other spherical Haar wavelet bases when the signals are approximated in the basis representation. The visual quality of reconstructed signals also affirms these results.

We briefly remark that in many applications such as environment map rendering in computer graphics, molecular electronic structure calculations in physics, and the alignment of spherical data sets in medical imaging, the rotation of spherical signals in their basis representation is necessary. Inspired by Wang et al. [2006], we have developed basis transformation matrices for spherical Haar wavelets bases [Lessig 2007]. These matrices permit the rotation of a signal in its basis representation. Unlike previous work, the matrices can be computed analytically. An analysis of their structure revealed that they are very sparse and quasi-block symmetric. This is important to compute rotations efficiently and to reduce otherwise significant matrix storage costs [Wang et al. 2006]. Experimental results demonstrated that the rotation in a spherically parametrized representation is significantly more efficient than that in a planar representation of the sphere such as those employed by Ng et al. [2003]. A more detailed discussion of rotation in spherical Haar wavelet bases, and more generally in Riesz bases, is beyond the scope of this paper. For further details see the work by Lessig [2007].[1]

2. RELATED WORK

Various representations for spherical signals have been proposed in the literature. *Spherical Harmonics* [MacRobert 1948] have been popular in physics and chemistry. The SH basis was also employed in other fields such as geoscience and medical imaging [Clarke et al. 2004; Katsuyuki et al. 2001]. In computer graphics, Spherical Harmonics have been used for example by Westin et al. [1992] to represent BRDFs, and Sillion et al. [1991] employed the basis for the representation of exitant radiance in offline radiosity computations. Cabral et al. [1987], and later Ramamoorthi and Hanrahan [2002], Kautz et al. [2002] and Sloan et al. [2002] used the SH basis for environment map rendering and Precomputed Radiance Transfer (PRT). In the past decade, Spherical Harmonics have been complemented by different spherical and hemispherical harmonic bases [Makhotkin 1996; Koenderink et al. 1996; Alfeld et al. 1996a; 1996b; Gautron et al. 2004; Sloan et al. 2005]. The global support of their basis functions, however, prevents harmonic bases from efficiently representing low-frequency signals. Wavelets, in contrast, are localized in both space and frequency and therefore efficient for the representation of all-frequency signals.

Spherical Radial Basis Functions have been used widely for example in astronomy and geoscience [Fisher et al. 1993; Narcowich and Ward 1996; Freeden et al. 1998; Freeden 1999]. Recently, these bases have also been employed in computer graphics [Green et al. 2006; Tsai and Shih 2006]. SRBFs are localized in both space

[1]An extended version of this work can be found Lessig's thesis, available online at `http://www.dgp.toronto.edu/~lessig/soho/data/msc_lessig.pdf`

and frequency and can thus efficiently represent all-frequency signals. In contrast to wavelets, however, obtaining the basis representation of a signal is prohibitively expensive [Green et al. 2006; Tsai and Shih 2006]. Furthermore, the unstructured nature of SRBF bases makes it difficult to develop efficient algorithms to process a signal in its basis representation. Such optimizations have shown to be efficient for wavelets [Ng et al. 2004; Sun and Mukherjee 2006].

Different wavelet representations for spherical signals exist in the literature. Lounsbery et al. [1997] defined wavelet bases over subdivision surfaces that can represent sphere-like shapes. Their construction can employ a wide range of subdivision schemes but none of the resulting bases is orthogonal. To make the bases practical it was additionally necessary to truncate the globally supported basis functions. Truncated basis functions, however, no longer form true wavelet bases.

Girardi and Sweldens [1997] developed orthogonal Haar wavelet bases over general measure spaces L_p. The scaling functions employed in their work are identical to those of the SOHO wavelet basis but their wavelet construction does not yield a symmetric basis on the sphere.

In their seminal work, Schröder and Sweldens [1995] proposed different vertex- and face-based spherical wavelets. Based on the work by Girardi and Sweldens [1997], the authors developed the *Bio-Haar* wavelets, a semi-orthogonal and symmetric spherical Haar wavelet basis. *Lifting* was used to obtain smooth, spherical wavelet bases. Schröder and Sweldens verified experimentally that the bases developed in their work are well suited for the representation of common spherical signals from computer graphics. An interesting side result of their experiments is that Haar-like wavelets are as efficient as smoother bases for the representation of image-like signals. This confirmed earlier theoretical results by Donoho [1993] that showed that Haar-like bases are close to optimal for the representation of functions of bounded variation. Ng et al. [2003] later provided similar results demonstrating that Haar-like wavelets are efficient for the representation of natural, all-frequency signals, and that these bases clearly outperform Spherical Harmonics.

Based on [Schröder and Sweldens 1995], Nielson et al. [1997], and later Bonneau [1999], developed semi-orthogonal, symmetric spherical Haar wavelet bases that are *nearly orthogonal*, in the sense that they become orthogonal in the limit as the subdivision level goes to infinity. Recently, Roşca [2005] likewise developed a family of nearly orthogonal spherical Haar wavelet bases. Unfortunately, none of these works provided detailed experimental results comparing their newly developed bases to incumbent spherical Haar wavelet bases.

Ma et al. [2006] used a Haar-like pseudo wavelet basis over the sphere for PRT. The basis is identical to that proposed by Bonneau [1999], but the authors assumed the subdivision of a partition yields child domains of equal area. This is in general not true and the *pseudo Haar wavelets* are therefore not a basis of the space $L_2(\mathbb{S}^2, d\omega)$ [Lessig 2007].

Wavelets parametrized over planar domains have also been used to represent spherical signals [Ng et al. 2003; 2004; Zhou et al. 2005; Wang et al. 2006; Sun and

Mukherjee 2006]. These techniques are limited in that a planar parametrization of the sphere unavoidably leads to distortion.

The SOHO wavelets are inspired by the bases developed by Schröder and Sweldens [1995] and by Bonneau [1999]. In contrast to these representations, our basis is both orthogonal and symmetric. Unlike Bonneau, we are also able to show that our new basis is an unconditional basis of the space $L_2(\mathbb{S}^2, d\omega)$ [Lessig 2007].

3. SECOND GENERATION WAVELETS

We shall present an overview of second generation wavelets, which provides the necessary background for the derivation of the SOHO wavelet basis in Section 4. A more comprehensive introduction may be found for example in Sweldens [1996] or Lessig [2007]. For brevity we also omit proofs in this section. The interested reader should consult the aforementioned references.

Second generation wavelets permit the representation of functions in L_2, the space of functions with finite energy, in a very general setting $L_2 \equiv L_2(X, \Sigma, \mu)$, where $X \subseteq \mathbb{R}^n$ is a spatial domain, Σ denotes a σ-algebra defined over X, and μ is a (possibly weighted) measure on Σ. Unlike first generation wavelets such as the Haar basis, the basis functions of second generation wavelets are no longer scales and translates of one particular mother basis function. Instead, a *multiresolution analysis* $\mathcal{M} = \{V_j \subset L_2 \mid j \in \mathcal{J} \subset \mathbb{Z}\}$ consisting of a sequence of nested subspaces V_j on different levels $j \in \mathcal{J}$ is employed to define the basis functions. $\mathcal{M}$ satisfies:

(1) $V_j \subset V_{j+1}$.

(2) $\bigcup_{j\in\mathcal{J}} V_j$ is dense in L_2.

(3) For every $j \in \mathcal{J}$, a Riesz basis of V_j is given by *scaling functions* $\{\varphi_{j,k} \mid k \in \mathcal{K}(j)\}$.

The $k \in \mathcal{K}(j)$ form a general index set defined over the scaling functions on level j. Next to the primary multiresolution analysis $\mathcal{M}$, also a dual multiresolution analysis $\tilde{\mathcal{M}} = \left\{\tilde{V}_j \mid j \in \mathcal{J} \subset \mathbb{Z}\right\}$ formed by the dual spaces $\tilde{V}_j$ exists. A basis of the $\tilde{V}_j$ is given by dual scaling functions $\tilde{\varphi}_{j,k}$. The scaling functions and their duals are *biorthogonal*:

$$\langle \varphi_{j,k} \ , \ \tilde{\varphi}_{j,k'} \rangle = \delta_{k,k'} \quad k, k' \in \mathcal{K}(j), \tag{1}$$

where $\langle f, g \rangle$ denotes an inner product on X, and $\delta_{k,k'}$ is the Kronecker delta. It follows from the nested structure of the spaces V_j that the scaling functions satisfy a refinement relationship:

$$\varphi_{j,k} = \sum_{l\in\mathcal{K}(j+1)} h_{j,k,l}\, \varphi_{j+1,l}, \tag{2}$$

where the $h_{j,k,l}$ are *scaling function filter coefficients*. An analogous relationship with dual scaling function filter coefficients $\tilde{h}_{j,k,l}$ holds for the $\tilde{\varphi}_{j,k}$. In the following it is assumed that all filters are of finite extent and uniformly bounded. This implies that finite index sets $\mathcal{L}(j,k) = \{l \in \mathcal{K}(j+1) \mid h_{j,k,l} \neq 0\}$ and $\mathcal{K}(j,l) = \{k \in \mathcal{K}(j) \mid h_{j,k,l} \neq 0\}$ exist. The index sets $\tilde{\mathcal{L}}(j,k)$ and $\tilde{\mathcal{K}}(j,l)$ for the dual scaling

function filter coefficients are defined analogously. Unless stated otherwise, l is assumed to run over $\mathcal{L}(j,k)$ or $\tilde{\mathcal{L}}(j,k)$, and k over $\mathcal{K}(j,l)$ or $\tilde{\mathcal{K}}(j,l)$.

A partition is used to define the scaling functions. A set of measurable subsets $\mathcal{S} = \{S_{j,k} \in \Sigma \mid j \in \mathcal{J},\ k \in \mathcal{K}(j)\}$ of X is a *partition* iff:

(1) $\forall j \in \mathcal{J}$: clos $\bigcup_{k\in\mathcal{K}(j)} S_{j,k} = X$ and the union is disjoint; that is for fixed j, the $S_{j,k}$ provide a simple cover of X.

(2) $\mathcal{K}(j) \subset \mathcal{K}(j+1)$.

(3) $S_{j+1,k} \subset S_{j,k}$.

(4) For a fixed $k_0 \in \mathcal{K}(j_0)$, $\bigcap_{j>j_0} S_{j,k_0}$ is a set containing exactly one point $x_0 \in X$.

Subdivision schemes for embeddings $X \subset \mathbb{R}^3$ such as the surface of a mesh are well-known examples of partitions.

The *wavelet basis functions* $\{\psi_{j,m} \mid j \in \mathcal{J},\ m \in \mathcal{M}(j)\}$ span the difference spaces W_j, with $V_j \oplus W_j = V_{j+1}$. A basis of W_j is thus given by all wavelet basis functions $\psi_{j,m}$ on level j, where the $m \in \mathcal{M}(j)$ form a general index set defined over the basis functions. It follows from the definition of the $\psi_{j,m}$ over the subspace $W_j \subset V_{j+1}$ that *wavelet basis function filter coefficients* $g_{j,m,l}$ exist with

$$\psi_{j,m} = \sum_{l\in\mathcal{K}(j+1)} g_{j,m,l}\ \varphi_{j+1,l}. \tag{3}$$

The dual wavelet basis functions $\tilde{\psi}_{j,m}$ span the difference spaces $\tilde{W}_j$, with $\tilde{V}_j \oplus \tilde{W}_j = \tilde{V}_{j+1}$, where the filter coefficients $\tilde{g}_{j,m,l}$ define the $\tilde{\psi}_{j,m}$ as linear combinations of the $\tilde{\varphi}_{j+1,l}$. As with the index sets defined for the scaling basis function filter coefficients, we also employ index sets that run over the non-zero filter coefficients of the wavelet basis functions. Unless stated otherwise, l is assumed to run over $\mathcal{L}(j,m)$ or $\tilde{\mathcal{L}}(j,m)$, and m over $\mathcal{M}(j,l)$ or $\tilde{\mathcal{M}}(j,l)$. The primary and dual wavelet basis functions are again biorthogonal:

$$\left\langle \psi_{j,k}\ ,\ \tilde{\psi}_{j',k'} \right\rangle = \delta_{j,j'}\,\delta_{k,k'} \quad \text{for} \quad k \in \mathcal{K}(j),\ k' \in \mathcal{K}(j'). \tag{4}$$

The biorthogonality of the basis functions can be propogated to the filter coefficients:

$$\begin{aligned} \textstyle\sum_l\ g_{j,m,l}\ \tilde{g}_{j,m',l} &= \delta_{m,m'} & \textstyle\sum_l\ h_{j,k,l}\ \tilde{g}_{j,m,l} &= 0 \\ \textstyle\sum_l\ h_{j,k,l}\ \tilde{h}_{j,k',l} &= \delta_{k,k'} & \textstyle\sum_l\ \tilde{h}_{j,k,l}\ g_{j,m,l} &= 0, \end{aligned} \tag{5}$$

for $j \in \mathcal{J}$, and all $k \in \mathcal{K}(j)$ and $m \in \mathcal{M}(j)$. A set of basis functions provides *perfect reconstruction* if the conditions in Eq. 5 hold, and

$$\sum_k h_{j,k,l}\ \tilde{h}_{j,k,l} + \sum_m g_{j,m,l}\ \tilde{g}_{j,m,l} = 1. \tag{6}$$

A *biorthogonal wavelet basis* Ψ can now be defined as

$$\Psi = \{\varphi_{0,0}\,,\ \psi_{j,m}\ \mid\ j \in \mathcal{J},\ m \in \mathcal{M}(j)\}\,,$$

where the basis functions provide perfect reconstruction. The primary basis functions of Ψ are denoted $\hat{\psi}_{j,m} \in \{\varphi_{0,0}, \psi_{j,m}\}$, and analogously $\check{\psi}_{j,m} \in \left\{\tilde{\varphi}_{0,0}, \tilde{\psi}_{j,m}\right\}$ for the dual basis functions. The second generation setting assumes biorthogonal wavelets. For orthogonal wavelet bases, the primary and dual basis functions coincide for all j and m [Schröder and Sweldens 1995], or, equivalently, every basis function is orthogonal to every other basis function [Stollnitz et al. 1996]. With $\varphi_{j,k} = \tilde{\varphi}_{j,k}$ and $\psi_{j,m} = \tilde{\psi}_{j,m}$, the second generation setting therefore also holds for orthonormal wavelet bases.

A function $f \in L_2$ can be represented in a wavelet basis as

$$f = \sum_i \left\langle f \,,\, \check{\psi}_i \right\rangle \hat{\psi}_i = \sum_i \gamma_i \hat{\psi}_i,$$

where the γ_i are the basis function coefficients, and $\mathcal{I}$ is a general index set defined over all basis functions of Ψ.

The *fast wavelet transform* is a pair of linear-time algorithms to project a signal into its basis representation and to reconstruct it by recursively applying analysis and synthesis steps, respectively. An *analysis step* of the fast wavelet transform is defined as

$$\lambda_{j,k} = \sum_l \tilde{h}_{j,k,l}\, \lambda_{j+1,l} \quad \text{and} \quad \gamma_{j,m} = \sum_l \tilde{g}_{j,m,l}\, \lambda_{j+1,l}, \tag{7}$$

computing the basis function coefficients at level j as a linear combination of the scaling function coefficients at level $j+1$. A *synthesis step* takes the form

$$\lambda_{j+1,l} = \sum_k h_{j,k,l}\, \lambda_{j,k} + \sum_m g_{j,m,l}\, \gamma_{j,m}, \tag{8}$$

reconstructing the scaling function coefficients at level $j+1$ from the basis function coefficients at level j.

4. SOHO WAVELETS

We now derive the SOHO wavelet basis. The basis spans the space $L_2 \equiv L_2(\mathbb{S}^2, d\omega)$ of functions with finite energy on the sphere. For the measure $d\omega$ we employ the standard area measure on $\mathbb{S}^2$, that is $d\omega \equiv d\omega(\theta, \phi) = \sin\theta \, d\theta \, d\phi$.

4.1 The Partition Scheme

The partition $\mathcal{T}$, over which the SOHO wavelet basis is defined, is formed by a set of spherical triangles $\mathcal{T} = \{T_{j,k} \mid j \in \mathcal{J}, k \in \mathcal{K}(j)\}$. The domains at the coarsest level $T_{0,k}$ are obtained by projecting a platonic solid with triangular faces such as the octahedron or the icosahedron onto the sphere. The domains at the next finer levels are formed by recursively subdividing every spherical triangle $T_{j,k}$ into four child triangles $T^k_{j+1,l}$. As shown in Fig. 1 (b), these are obtained by inserting one new vertex $v^l_{j,k}$ on each of the arcs forming the sides of the $T_{j,k}$. It follows from the subdivision scheme that $\mathcal{T}$ is formed by a forest of partition trees and the domains $T_{0,k}$ at the coarsest level are the root nodes of these trees.

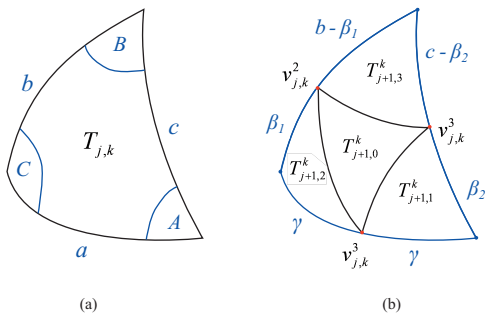

Fig. 1. Subdivision of a spherical triangle. The labeling of the entities of a spherical triangle $T_{j,k}$ is shown in (a), the 4-fold subdivision yielding the child triangles in (b).

Although $\mathcal{T}$ is defined similarly to the partition used by Schröder and Sweldens [1995] we do not employ the geodesic bisector to obtain the positions of the new vertices $v^l_{j,k}$. For the SOHO wavelet basis, the vertex positions are chosen so that the *areas* of the three outer child triangles $T^k_{j+1,1}$, $T^k_{j+1,2}$, and $T^k_{j+1,3}$ are equal. This is the key to the derivation of a basis that is both orthogonal and symmetric. The novel subdivision scheme employed in our work will be detailed in Section 4.4.

The area of a spherical triangle $T_{j,k}$ will be denoted $\alpha_{j,k}$, and we define $\tau_{j,k} \equiv \tau_{j,k}(\omega)$ to be the characteristic (or indicator) function of $T_{j,k}$.

4.2 Scaling Basis Functions

For a Haar-like basis, the scaling basis functions $\varphi_{j,k}$ are constant over their support $T_{j,k}$ and thus defined as

$$\varphi_{j,k} = \eta_{j,k}\, \tau_{j,k},$$

where $\eta_{j,k}$ is a normalization constant chosen to satisfy Eq. 1. With $\eta_{j,k} = 1/\sqrt{\alpha_{j,k}}$, it follows immediately from the disjoint nature of the $T_{j,k}$ for fixed j that the $\varphi_{j,k}$ on the same level are orthogonal as required in Eq. 1. The scaling functions for the SOHO wavelet basis are thus

$$\varphi_{j,k} = \frac{\tau_{j,k}}{\sqrt{\alpha_{j,k}}}. \tag{9}$$

Given the $\varphi_{j,k}$, the filter coefficients $h_{j,k,l}$ must be chosen to satisfy Eq. 2. It follows from the partition that $\#\mathcal{L}(j,k) = 4$ and that the union of the child domains $\tau^k_{j+1,l}$ is again $\tau_{j,k}$. The filter coefficients are therefore

$$h_{j,k,l} = \frac{\sqrt{\alpha^k_{j+1,l}}}{\sqrt{\alpha_{j,k}}}. \tag{10}$$

For the partition $\mathcal{T}$ and the filter coefficients $h_{j,k,l}$ in Eq. 10, the *cascade algorithm* converges to the scaling functions in Eq. 9 [Lessig 2007]. This is a necessary condition for the existence of a wavelet basis.

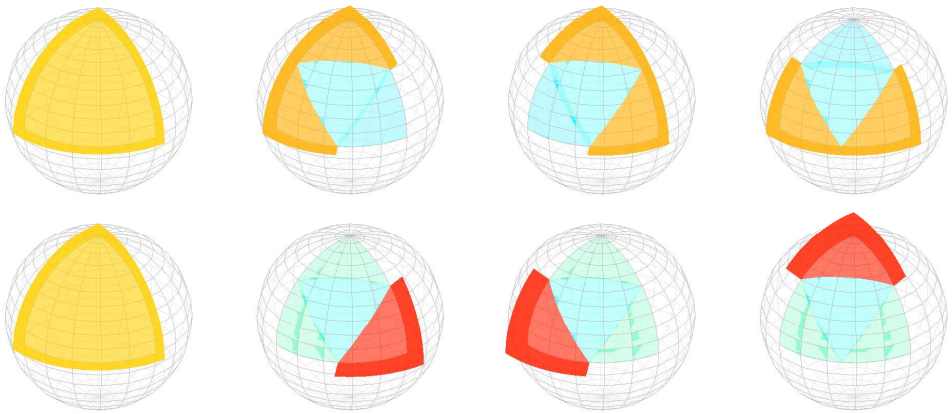

Fig. 2. The scaling basis function and the two possible sets of wavelet basis functions defined over a partition at level 0. The top row shows the basis functions where the positive sign has been employed in the computation of parameter a in Eq. 15, the bottom row shows the basis functions where the negative sign has been used. The basis is defined over a partition derived from an octahedron. Reddish hues indicate positive filter coefficients, bluish hues negative ones.

4.3 Wavelet Basis Functions

We use a custom two-step approach to derive the wavelet basis functions: In the first step a semi-orthogonal basis is developed, and in the second step orthogonality and symmetry are enforced.

For a Haar-like basis, the wavelet basis functions $\psi^l_{j,k}$, with $l = 0, 1, 2$, associated with a partition $T_{j,k}$ are exclusively defined over the child partitions $T^k_{j+1,l}$. All wavelet basis functions $\psi^{l_1}_{j,k_1}$ and $\psi^{l_2}_{j,k_2}$ defined on the same level j but over different partitions $k_1 \neq k_2$ are thus trivially orthogonal. For $\left\langle \psi^{l_1}_{j_1,k_1}, \psi^{l_2}_{j_2,k_2} \right\rangle = 0$ with $j_1 \neq j_2$ to be true, we require that the wavelet basis functions have a vanishing integral. It is easy to show that for a Haar-like basis this in fact implies that the wavelet basis functions on different levels are orthogonal [Lessig 2007].

In the following it is therefore sufficient to consider only one spherical triangle $T_{j,k}$, with fixed but arbitrary j and k, together with its child triangles $T^k_{j+1,l}$, for the derivation of the wavelet basis functions (cf. [Bonneau 1999]). The areas of interest will be abbreviated $\alpha_l \equiv \alpha^k_{j+1,l}$ and $\alpha_p \equiv \alpha_{j,k}$; analogous notation will be used for the characteristic functions $\tau_{j,k}$. In some cases we will also omit the indices j and k. It is then understood that these are the fixed j and k of $T_{j,k}$.

Considering only one partition $T_{j,k}$, the analysis and synthesis steps in Eq. 7 and Eq. 8 can be expressed as compact matrix-vector products. Perfect reconstruction requires that the analysis and synthesis matrices $A_{j,k}$ and $S_{j,k}$, respectively, satisfy $A_{j,k} = S^{-1}_{j,k}$; for an orthonormal basis this simplifies to $A_{j,k} = S^T_{j,k}$. A synthesis step in matrix-vector notation is of the form

$$\begin{pmatrix} \lambda_{j+1,0} \\ \lambda_{j+1,1} \\ \lambda_{j+1,2} \\ \lambda_{j+1,3} \end{pmatrix} = \begin{pmatrix} h_0 & g_0^0 & g_0^1 & g_0^2 \\ h_1 & g_1^0 & g_1^1 & g_1^2 \\ h_2 & g_2^0 & g_2^1 & g_2^2 \\ h_3 & g_3^0 & g_3^1 & g_3^2 \end{pmatrix} \begin{pmatrix} \lambda_j \\ \gamma_j^0 \\ \gamma_j^1 \\ \gamma_j^2 \end{pmatrix}, \tag{11}$$

where g_l^i denotes the l^{th} filter coefficient associated with the i^{th} wavelet basis function $\psi_{j,k}^i$ defined over $T_{j,k}$, and the h_l are the filter coefficients derived in Section 4.2.

We have already discussed the advantages of symmetric bases but have not yet provided a proper definition: Given a partition $T_{j,k}$, a spherical Haar wavelet basis is *symmetric* if the labeling of the child triangles $T_{j+1,1}^k$, $T_{j+1,2}^k$, and $T_{j+1,3}^k$ can be altered without changing the numerical values of the basis function coefficients associated with $T_{j,k}$.

In the following we will derive a semi-orthogonal spherical Haar wavelet basis. For fixed $T_{j,k}$, a biorthogonal wavelet basis is *semi-orthogonal* if it satisfies

$$\left\langle \psi_{j,k}^0 \, , \, \varphi_{j,k} \right\rangle = \left\langle \psi_{j,k}^1 \, , \, \varphi_{j,k} \right\rangle = \left\langle \psi_{j,k}^2 \, , \, \varphi_{j,k} \right\rangle = 0. \tag{12}$$

Eq. 12 can be written in Dirac bra-ket notation:

$$[\langle \Phi_j \mid \Psi_j \rangle] = 0, \tag{13}$$

where $[\langle X \mid Y \rangle]$ denotes the matrix of inner products of the two function sets X and Y, and Φ_j and Ψ_j are matrices containing the scaling and wavelet basis functions defined over $T_{j,k}$, respectively. Eq. 13 can be expanded with the refinement relationship in Eq. 3 [Stollnitz et al. 1996; Finkelstein and Salesin 1994] yielding

$$[\langle \Phi_j \mid \Phi_{j+1} \rangle] \, G_j = 0.$$

The matrix Φ_j is degenerate, containing only $\varphi_{j,k}$; Φ_{j+1} is formed by the four scaling functions $\varphi_{j+1,l}^k$ defined over the child domains $T_{j+1,l}^k$; and G_j contains the desired wavelet basis function filter coefficients g_l^i. The matrix G_j spans the nullspace of $[\langle \Phi_j \mid \Phi_{j+1} \rangle]$ and is obtained using existing techniques, giving

$$G_j = \begin{bmatrix} -\frac{\sqrt{\alpha_1}}{\sqrt{\alpha_0}} & -\frac{\sqrt{\alpha_2}}{\sqrt{\alpha_0}} & -\frac{\sqrt{\alpha_3}}{\sqrt{\alpha_0}} \\ 1 & 0 & 0 \\ 0 & 1 & 0 \\ 0 & 0 & 1 \end{bmatrix}. \tag{14}$$

It is easy to show that the wavelet basis functions defined in Eq. 14 have a vanishing integral [Lessig 2007].

Given the semi-orthogonal basis derived above, we now have to enforce symmetry and orthogonality of the wavelet basis functions, while taking care to preserve the properties that have already been established. Let $\hat{S}_{j,k}$ be a synthesis matrix formed by the h_l and g_l^i derived previously. We first tried to augment each of

the wavelet basis function filter coefficients g_l^i in $\hat{S}_{j,k}$ with a free parameter. The desired properties of the basis could then be formulated as a linear system, and the solution to the system would be the wavelet basis functions. However, we were not able to find such a solution and in fact a solution to the system might not exist.

To obtain a basis having the desired properties we instead required that the area of the three outer child partitions $T^k_{j+1,1}$, $T^k_{j+1,2}$, and $T^k_{j+1,3}$ of $T_{j,k}$ be equal (cf. Fig. 1); in Section 4.4 it will be shown that the partition $\mathcal{T}$ can be constructed so that this constraint is satisfied. With the area-isometry of the three outer child triangles, symmetry can be guaranteed by the following parametrization of the synthesis matrix:

$$\hat{S}_{j,k} = \begin{bmatrix} \frac{\sqrt{\alpha_0}}{\sqrt{\alpha_p}} & -c\frac{\sqrt{\alpha_1}}{\sqrt{\alpha_0}} & -c\frac{\sqrt{\alpha_1}}{\sqrt{\alpha_0}} & -c\frac{\sqrt{\alpha_1}}{\sqrt{\alpha_0}} \\ \frac{\sqrt{\alpha_1}}{\sqrt{\alpha_p}} & b & a & a \\ \frac{\sqrt{\alpha_1}}{\sqrt{\alpha_p}} & a & b & a \\ \frac{\sqrt{\alpha_1}}{\sqrt{\alpha_p}} & a & a & b \end{bmatrix},$$

where a, b, and c are the remaining free parameters. Enforcing orthogonality of the basis then yields a simple linear system whose solution are the wavelet basis functions for the SOHO wavelet basis (cf. Appendix A):

$$\begin{aligned} \psi^0_{j,k} &= \frac{\Lambda_1}{\Lambda_0}\tau_0 + \frac{1}{\Lambda_1}(\,(-2a+1)\,\tau_1 + a\,\tau_2 + a\,\tau_3) \\ \psi^1_{j,k} &= \frac{\Lambda_1}{\Lambda_0}\tau_0 + \frac{1}{\Lambda_1}(\,a\,\tau_1 + (-2a+1)\,\tau_2 + a\,\tau_3) \\ \psi^2_{j,k} &= \frac{\Lambda_1}{\Lambda_0}\tau_0 + \frac{1}{\Lambda_1}(\,a\,\tau_1 + a\,\tau_2 + (-2a+1)\,\tau_3), \end{aligned}$$

where

$$a = \frac{\alpha_0 \pm \sqrt{\alpha_0^2 + 3\,\alpha_0\,\alpha_1}}{3\alpha_0} \tag{15}$$

and $\Lambda_l \equiv \sqrt{\alpha^k_{j+1,l}}$. The two solutions for parameter a yield two different sets of wavelet basis functions. These are shown in Fig. 2. The area measures α_0 and α_1 are always positive and thus a is guaranteed to be real for both solutions.

Given the orthogonal basis derived above, an orthonormal basis can be obtained by normalizing the wavelet basis functions. Lessig [2007] further establishes that the SOHO wavelets form an unconditional basis of the space $L_2(\mathbb{S}^2, d\omega)$.

4.4 Construction of the Partition

The previous section demonstrated that the SOHO wavelet basis can be constructed provided the three outer child triangles $T^k_{j+1,1}$, $T^k_{j+1,2}$, and $T^k_{j+1,3}$ of $T_{j,k}$ have equal area. The geodesic bisector subdivision employed by Schröder and Sweldens [1995] does not have this property. The partition $\mathcal{T}$, as defined in Section 4.1, only imposes

Subdivision Scheme	Octahedron		Icosahedron	
Level	5	7	5	7
Our subdivision	43.0864	43.0417	53.5981	53.5808
Geodesic midpoint	45.0345	45.0022	54.0163	54.0010

Table I. Shape distortion for the partition proposed in this work and the geodesic bisector subdivision employed by Schröder and Sweldens. The minimum internal angle (in degrees) over all partitions was used as distortion measure.

a topology (cf. [Nielson et al. 1997]). The vertices $v^l_{j,k}$ can therefore be positioned so that $\alpha_1 = \alpha_2 = \alpha_3$. Let $v^1_{j,k}$ still be the geodesic bisector. The positions of $v^2_{j,k}$ and $v^3_{j,k}$ can then be obtained with a system of equations:

$$\begin{aligned}
\cot\left(\frac{E}{2}\right) &= \cot(C) + \frac{\cot\left(\frac{1}{2}\beta_1\right)\cot\left(\frac{1}{2}\gamma\right)}{\sin(C)} \\
\cot\left(\frac{E}{2}\right) &= \cot(B) + \frac{\cot\left(\frac{1}{2}\beta_2\right)\cot\left(\frac{1}{2}\gamma\right)}{\sin(B)} \\
\cot\left(\frac{E}{2}\right) &= \cot(A) + \frac{\cot\left(\frac{1}{2}b - \frac{1}{2}\beta_1\right)\cot\left(\frac{1}{2}c - \frac{1}{2}\beta_2\right)}{\sin(A)},
\end{aligned}$$

where we employed Eq. 36 from Todhunter's book [1901] to define the system. The variables on the right hand side of the equations are given in Fig. 1, and E denotes the spherical excess of the three outer child domains. Solving the system for β_1 and β_2 yields the desired vertex positions. The resulting formulae are lengthy and may be found in Appendix B. Lessig [2007] establishes that with a consistent labeling of $T_{j,k}$ exactly one solution for the area equality exists.

For the partition $\mathcal{T}$ it is desirable to yield spherical triangles that are uniform. We have not yet been able to prove bounds on the shape distortion introduced by our new subdivision. Numerical experiments show however that it is not significantly larger than for the geodesic bisector subdivision employed by Schröder and Sweldens [1995]. We used the minimum internal angle over all partitions to measure the shape distortion. The results are given in Table I.

5. EXPERIMENTAL EVALUATION

The performance of a basis depends on a variety of factors and superior theoretical properties are no guarantee of better results in practice. We therefore performed a variety of experiments to assess the practical efficacy of the SOHO wavelet basis. To provide insights for a wide range of applications we focused on experiments which are independent of specific settings.

5.1 Methodology

In the experiments the SOHO wavelet basis has been compared to six previously proposed spherical Haar wavelet bases: the Bio-Haar basis developed by Schröder and Sweldens [1995], the two nearly orthogonal bases proposed by Nielson et al. [1997], the pseudo Haar wavelets used by Ma et al. [2006], and the two nearly

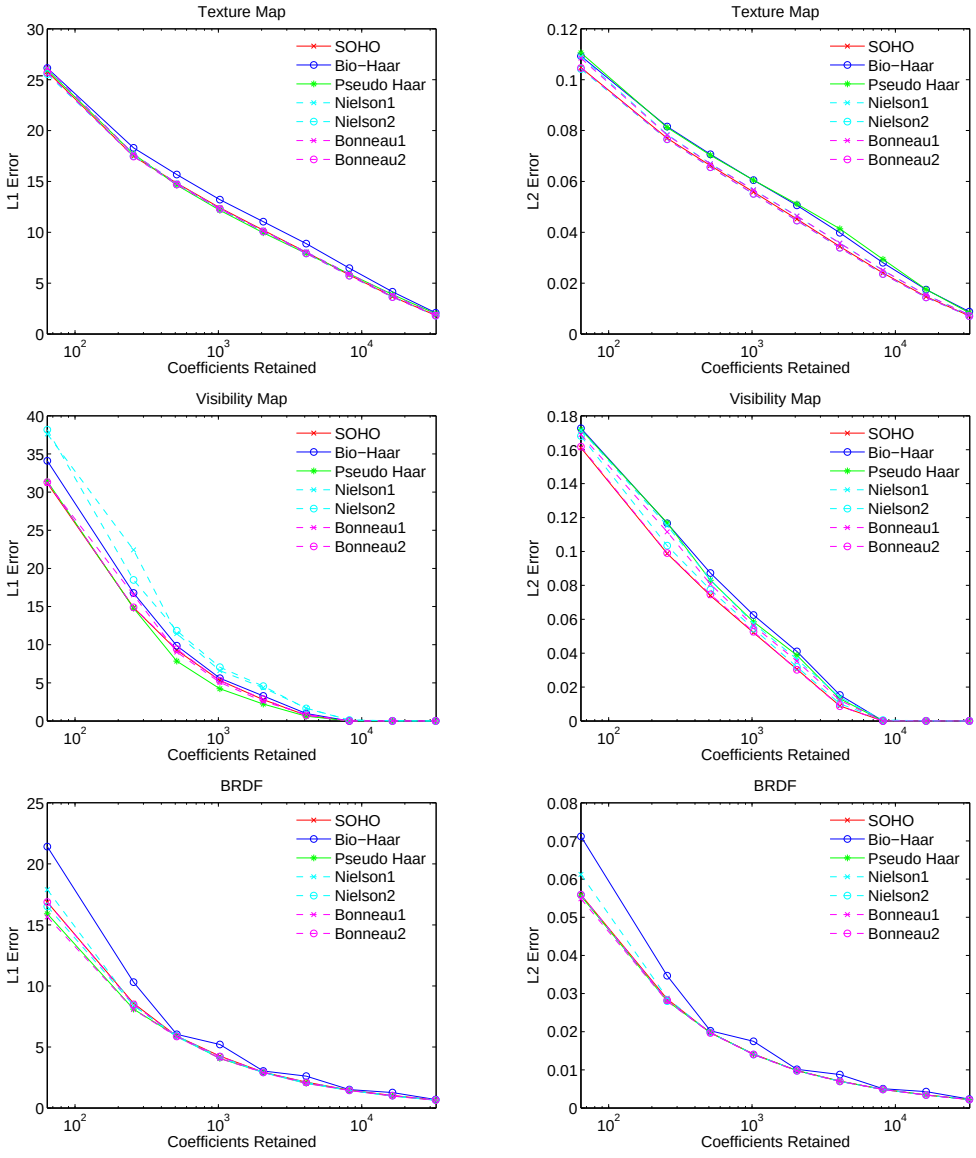

Fig. 3. Area-corrected error rates in the ℓ_1 and ℓ_2 norm for approximations of the test signals. The total number of basis function coefficients of the signals was $131,072$.

orthogonal bases developed by Bonneau [1999]. All bases have been employed to represent three signals: a unimodal function with only low-frequency content, a piecewise constant function with only high-frequency features, and an image-like signal with content in the full frequency spectrum. For convenience we will refer to the test signals as *BRDF*, *visibility map*, and *texture map*, respectively (cf. Fig. 4).

When a signal is represented in a wavelet basis, typically a large proportion of the basis function coefficients is very small or zero, and a small number of coefficients is sufficient to obtain reconstructions that closely resemble the original signal. In the experiments we therefore investigated the connection between the error in reconstructed signals and the number of basis function coefficients used to obtain the reconstructions. As error measures we employed the ℓ_1 and the ℓ_2 norm. In the literature it has been argued that for images the ℓ_1 norm better corresponds to the perceived image quality than other numerical error measures [DeVore et al. 1992]. Our test signals can been seen as images on the sphere and we therefore wanted to explore whether or not the ℓ_1 norm is in fact a more appropriate error measure for the signals than the ℓ_2 norm which is the standard norm for the space $L_2(\mathbb{S}^2, d\omega)$. Numerical error measures are valuable in many contexts but they are limited in their ability to measure the quality of a signal as it is perceived by humans [Pratt 1991]. In Fig. 4 we therefore provide plots of reconstructed signals.

The problem of finding the optimal approximation in a basis representation, that is the set of basis function coefficients which minimizes the reconstruction error for a fixed number k of coefficients employed for an approximation, is in general considered to be very hard (cf. [Gross 1996]). Only with the ℓ_2 norm and for an orthogonal basis is it possible to efficiently obtain the optimal approximation: in this case in fact the k largest basis function coefficients yield the minimal reconstruction error. One of the motivations for the development of nearly orthogonal spherical Haar wavelet bases was to obtain representations which show in practice the same behavior as orthogonal bases. Following a similar idea, Ma et al. likewise assumed that the pseudo Haar wavelets provide the same benefits as orthogonal bases. We thus employed the ℓ_2 optimal approximation strategy for orthogonal bases not only for the SOHO wavelet basis but also for the nearly orthogonal Haar wavelets and the pseudo Haar basis. For the semi-orthogonal Bio-Haar basis the approximation given by the k largest basis function coefficients is far from optimal [Lessig 2007]. For this basis we therefore employed the ℓ_2 optimal approximation strategy as derived in [Lessig 2007], disregarding the fact that the computations are significantly more expensive than for the other bases.

5.2 Evaluation of Approximation Performance

As shown in Fig. 2, two different SOHO wavelet bases can be obtained by either using the positive or the negative sign in the computation of parameter a in Eq. 15. In the experiments the basis in which the negative sign had been employed performed slightly better and in the remainder of the paper we will therefore refer to this basis as the SOHO wavelet basis.

The subdivsion scheme proposed in Section 4.4 allows the SOHO wavelet basis to

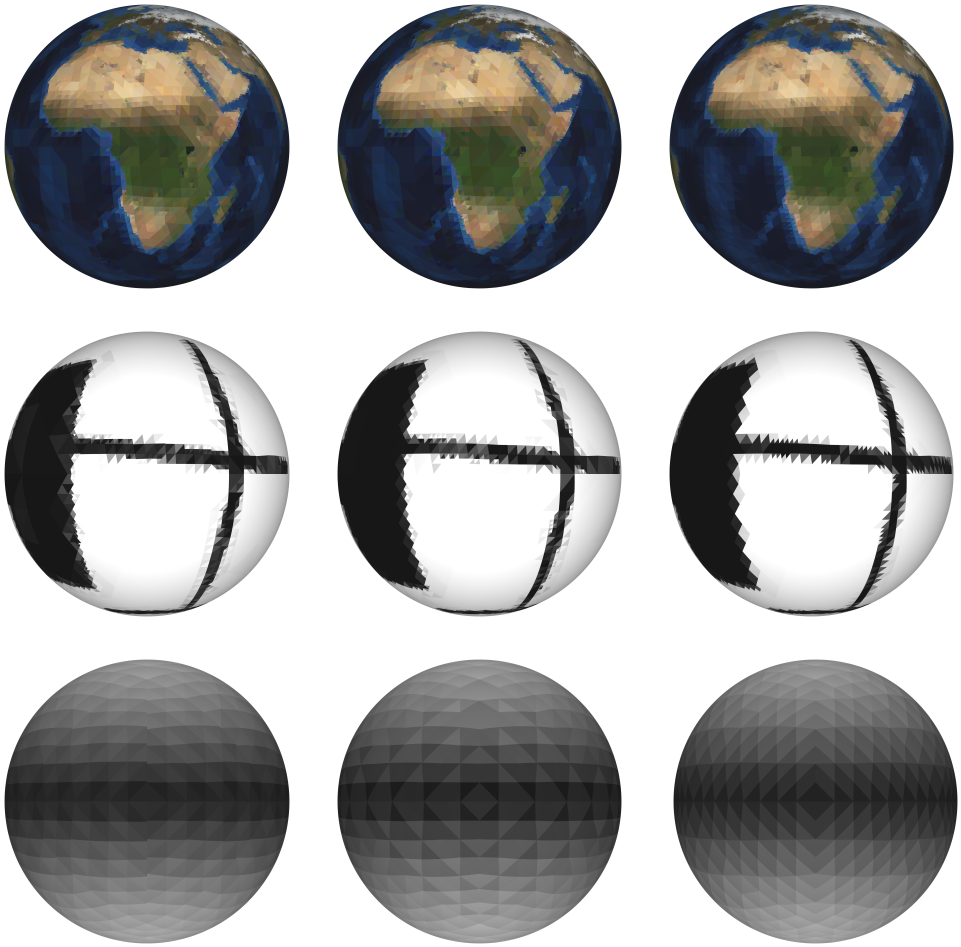

Fig. 4. Reconstructed signals for the SOHO wavelet basis, the Bio-Haar basis, the pseudo Haar basis (from left to right).

be defined over a partition derived from a tetrahedron, an octahedron, or an icosahedron. Although in our experiments none of the resulting bases provided a clear advantage, we argue that in general the octahedron is the best choice for the base polyhedron. The basis induced by the octahedron never yielded the highest error rate in any of our experiments and it can directly represent hemispherical signals. The alignment of a partition derived from an octahedron with other parametrizations of the sphere is in addition useful in many applications. In the experiments discussed in the following we always employed the octahedron as base polyhedron.

For the spherical Haar wavelet bases employed in the experiments, in Fig. 3 the error rates in the ℓ_1 and the ℓ_2 norm resulting from an approximation of the test signals with an increasing number of nonzero basis function coefficients are shown. The basis Bonneau2 performed for all signals very similarly to the SOHO wavelet

basis and in the plots both representations are in most cases indistinguishable. For the visibility map the basis Bonneau1 provided higher error rates than the SOHO wavelet basis; both bases achieved however very similar results for the other two signals. The two bases developed by Nielson et al. provided for the texture map almost the same error rates as the SOHO wavelet basis; for the visibility map however, in particular in the ℓ_1 norm, the error rates were higher. For the BRDF, the basis Nielson2 performed slightly better than the SOHO wavelet basis whereas the basis Nielson1 obtained inferior results. With the exception of the BRDF where the pseudo Haar basis achieved similar results than the SOHO wavelets, the Bio-Haar basis and the pseudo Haar wavelets provided always higher error rates than the other bases. Note that independent of the basis for the visibility map about 5% of the basis function coefficients were sufficient to provide reconstructions with virtually no error. The full information of the signal could therefore be represented with a small fraction of all coefficients.

In Fig. 4 reconstructions of the test signals with a subset of all basis function coefficients are shown. The plots for the SOHO wavelet basis look in most cases very similar to those of the nearly orthogonal bases and we therefore provide reconstructions only for the SOHO wavelet basis, the Bio-Haar basis, and the pseudo Haar wavelets. For the texture map we employed 8 192, or 6.25%, of the original 131 072 basis function coefficients for reconstruction, for the other two signals 1 024, or 0.78%, of the coefficients were retained. Although the perceived quality is an inherently subjective measure, we argue that the SOHO wavelet basis achieved for all signals visually more pleasing results than the other two bases shown in the comparison. For the texture map the SOHO wavelet basis provides sharper edges and the reconstructed signal appears less noisy. The basis also preserves more details which can be seen for example in the center of Africa where only for the SOHO wavelet basis are the two lakes south of Lake Victoria clearly visible. For the BRDF, the reconstructed signal for the SOHO wavelet basis appears significantly smoother than the reconstructions for the Bio-Haar basis and the pseudo Haar wavelets, and it therefore better resembles the original Lambertian BDRFs. For the visibility map, the SOHO wavelet basis provides again sharper edges than the other two bases.

5.3 Discussion

We believe that the presented results provide valuable insights about the strengths and weaknesses of spherical Haar wavelets and in particular of the SOHO wavelet basis. Some experiments have been omitted as the results have already been presented in previous work. Ng et al. [2003] for example showed that Haar-like bases are significantly more efficient than Spherical Harmonics for the representation of all-frequency functions, and Schröder and Sweldens [1995] demonstrated that spherical Haar wavelet bases are as efficient as smoother, spherical wavelets for the representation of image-like signals.

The results shown in Fig. 3 demonstrate that the error rates in the ℓ_1 and the ℓ_2 norm are highly correlated, resembling earlier observations by Schröder and Sweldens [1995]. A similar correlation can be observed between both numerical er-

ror measures employed in our experiments and the visual quality of reconstructed signals; this contradicts DeVore et al. [1992] who argued that the ℓ_1 error norm better corresponds to the visual quality of image-like signals than other numerical error measures. In applications it is thus possible to employ the ℓ_2 norm to accurately estimate the error in the ℓ_1 norm or the visual quality of reconstructed signals. This is important as only for the ℓ_2 norm is it easy to find the optimal approximation, in log-linear time for orthogonal bases and still at moderate costs for many other practically relevant bases.

It is well-known that Haar-like bases are well suited for the representation of piecewise constant functions such as visibility maps. The experiments presented in this section demonstrate, however, that these bases are also efficient for the representation of smooth signals. For the BRDF for example 0.78% of all basis function coefficients were sufficient to provide visually pleasing reconstructions as shown in Fig. 4. The texture map has features in the full frequency spectrum and thus more basis function coefficients had to be retained. Reconstructions which closely resemble the original signal could however still be obtained with not more than 5% of the basis function coefficients.

Prior to the experiments, we had anticipated that the nearly orthogonal spherical Haar wavelet bases would outperform the Bio-Haar and the pseudo Haar wavelets. That these bases provided results very similar to those of the SOHO wavelet basis was however surprising to us. We initially thought that this might result from the high subdivision level on which the signals were defined so that the bases already approached their limit properties. Additional experiments showed however that the good performance of the nearly orthogonal spherical Haar wavelet bases is independent of the resolution of the input signal, hinting that the design of the basis functions rather than the nearly orthogonality of the bases causes the results. It will be interesting to explore how the nearly orthogonal bases perform for other applications where orthogonality is of importance.

Considering that the pseudo Haar wavelets are not a basis of $L_2(\mathbb{S}^2, d\omega)$ it was surprising to us that the representation provided for almost all of the experiments results competitive to those of the true spherical Haar wavelet bases. The assumption that the geodesic bisector subdivision yields child domains with equal area seems therefore in practice to be reasonable. For applications the pseudo Haar wavelets provide the advantage that the filter coefficients are constant and do not depend on the area of the domains of the partition.

5.4 Costs of Wavelet Transform

For spherical Haar wavelet bases it is expensive to compute the partition and the filter coefficients which are necessary to perform wavelet transforms. For the SOHO wavelet basis additional costs result from our novel subdivision scheme. Both the partition and the filter coefficients can however be precomputed so that the costs of performing wavelet transforms are independent of the basis and similar to those of wavelets in $2D$.

6. FUTURE WORK

We believe that many applications might benefit from the use of the SOHO wavelet basis. In computer graphics, for example the solution of the rendering equation [Kajiya 1986] is likely to be more efficient with a representation of the factors of the product integral equation in the SOHO wavelet basis. The light transport factors in this case are usually not aligned and have to be rotated before a solution can be obtained efficiently. It would be interesting to explore the possibility of computing basis transformation matrices for these rotations at runtime, thereby avoiding approximations and reducing the otherwise significant storage requirements [Wang et al. 2006].

Beyond computer graphics, applications for example in medical imaging, astrophysics, and geoscience might benefit from the use of the SOHO wavelet basis. In medical imaging in particular the orthonormality of the basis will be of interest; for example the ability to rigorously establish error bounds. For the very large data sets in astrophysics and geoscience the superior approximation performance of the SOHO wavelet basis will be beneficial.

Some theoretical questions also remain. In this work we derived an orthogonal and symmetric spherical Haar wavelet basis by requiring area-isometry of the three outer child partitions. The question if such a basis exists without the area constraint is still unanswered. Another open problem is if smooth, orthogonal and symmetric wavelets on $\mathbb{S}^2$ exist, and if such a basis provides practical advantages over the SOHO wavelet basis.

7. CONCLUSION

In this work we developed the SOHO wavelet basis, a novel spherical Haar wavelet basis that is both orthogonal and symmetric, contradicting previous work that doubted the existence of such a basis. Experimental results verify that the superior theoretical properties of the SOHO wavelet basis are also of practical relevance.

Combining the findings of this paper, we believe that the SOHO wavelet basis is an attractive representation for the approximation and processing of all-frequency signals on the sphere, and we anticipate that the basis will enable more efficient solutions for many problems in computer graphics and beyond.

8. ACKNOWLEDGEMENT

We would like to thank Silvio Boraç for providing early feedback on our work and Michael Daum for his help on editing the paper.

REFERENCES

Alfeld, P., Neamtu, M., and Schumaker, L. L. 1996a. Bernstein-Bézier Polynomials on Spheres and Sphere-like Surfaces. *Computer Aided Geometric Design 13,* 4, 333–349.

Alfeld, P., Neamtu, M., and Schumaker, L. L. 1996b. Fitting Scattered Data on Sphere-like Surfaces using Spherical Splines. *J. Comput. Appl. Math. 73,* 1-2, 5–43.

Bonneau, G.-P. 1999. Optimal Triangular Haar Bases for Spherical Data. In *VIS '99: Proceedings of the Conference on Visualization '99*. IEEE Computer Society Press, Los Alamitos, CA, USA, 279–284.

Cabral, B., Max, N., and Springmeyer, R. 1987. Bidirectional Reflection Functions from Surface Bump Maps. In *SIGGRAPH '87: Proceedings of the 14th Annual Conference on Computer Graphics and Interactive Techniques*. ACM Press, New York, NY, USA, 273–281.

Clarke, P. J., Lavalee, D. A., Blewitt, G., and van Dam, T. 2004. Choice of Basis Functions for the Representation of Seasonal Surface Loading Signals in Geodetic Time Series. *AGU Fall Meeting Abstracts*, A121+.

DeVore, R. A., Jawerth, B., and Lucier, B. J. 1992. Image Compression through Wavelet Transform Coding. *IEEE Transactions on Information Theory 38,* 2, 719–746.

Donoho, D. L. 1993. Unconditional Bases are Optimal Bases for Data Compression and Statistical Estimation. *Appl. Comp. Harm. Anal. 1*, 100–115.

Finkelstein, A. and Salesin, D. H. 1994. Multiresolution Curves. In *SIGGRAPH '94: Proceedings of the 21st annual Conference on Computer Graphics and Interactive Techniques*. ACM Press, New York, NY, USA, 261–268.

Fisher, N. I., Lewis, T., and Embleton, B. J. J. 1993. *Statistical Analysis of Spherical Data*. Cambridge University Press.

Freeden, W. 1999. *Multiscale Modelling of Spaceborne Geodata*. B.G. Teubner, Stuttgart, Leipzig.

Freeden, W., Gervens, T., and Schreiner, M. 1998. *Constructive Approximation on the Sphere (With Applications to Geomathematics)*. Oxford Sciences Publication. Clarendon Press, Oxford University.

Gautron, P., Křivánek, J., Pattanaik, S. N., and Bouatouch, K. 2004. A Novel Hemispherical Basis for Accurate and Efficient Rendering. In *Rendering Techniques 2004, Eurographics Symposium on Rendering*. 321–330.

Girardi, M. and Sweldens, W. 1997. A New Class of Unbalanced Haar Wavelets that form an Unconditional Basis for L_p on General Measure Spaces. *J. Fourier Anal. Appl. 3,* 4.

Green, P., Kautz, J., Matusik, W., and Durand, F. 2006. View-Dependent Precomputed Light Transport using Nonlinear Gaussian Function Approximations. In *SI3D '06: Proceedings of the 2006 Symposium on Interactive 3D Graphics and Games*. ACM Press, New York, NY, USA, 7–14.

Gross, M. H. 1996. L2 Optimal Oracles and Compression Strategies for Semiorthogonal Wavelets.

Kajiya, J. T. 1986. The Rendering Equation. In *SIGGRAPH '86: Proceedings of the 13th Annual Conference on Computer Graphics and Interactive Techniques*. ACM Press, New York, NY, USA, 143–150.

Katsuyuki, T., Gengsheng, L. Z., and Gullberg, G. T. 2001. Cone-Beam Image Reconstruction using Spherical Harmonics. *Physics in Medicine and Biology 46*, N127–N138(1).

Kautz, J., Sloan, P.-P., and Snyder, J. 2002. Fast, Arbitrary BRDF Shading for Low-Frequency Lighting using Spherical Harmonics. In *EGRW '02: Proceedings of the 13th Eurographics Workshop on Rendering*. Eurographics Association, Aire-la-Ville, Switzerland, Switzerland, 291–296.

Koenderink, J. J., van Doorn, A. J., and Stavridi, M. 1996. Bidirectional Reflection Distribution Function Expressed in Terms of Surface Scattering Modes. In *ECCV '96: Proceedings of the 4th European Conference on Computer Vision-Volume II*. Springer-Verlag, London, UK, 28–39.

Lessig, C. 2007. Orthogonal and Symmetric Wavelets on the Sphere.

Lounsbery, M., DeRose, T. D., and Warren, J. 1997. Multiresolution Analysis for Surfaces of Arbitrary Topological Type. *ACM Trans. Graph. 16,* 1, 34–73.

Ma, W.-C., Hsiao, C.-T., Lee, K.-Y., Chuang, Y.-Y., and Chen, B.-Y. 2006. Real-Time Triple Product Relighting Using Spherical Local-Frame Parameterization. *The Visual Computer* 9-11, 682–692. Pacific Graphics 2006 Conference Proceedings.

MacRobert, T. M. 1948. *Spherical Harmonics; An Elementary Treatise on Harmonic Functions, with Applications*. Dover Publications.

Makhotkin, O. A. 1996. Analysis of Radiative Transfer between Surfaces by Hemispherical Harmonics. *Journal of Quantitative Spectroscopy and Radiative Transfer 56*, 869–879.

Narcowich, F. J. and Ward, J. D. 1996. Nonstationary Wavelets on the m-Sphere for Scattered Data. *App. Comput. Harm. Anal. 3*, 324–336.

Ng, R., Ramamoorthi, R., and Hanrahan, P. 2003. All-Frequency Shadows using Non-Linear Wavelet Lighting Approximation. *ACM Trans. Graph. 22,* 3, 376–381.

Ng, R., Ramamoorthi, R., and Hanrahan, P. 2004. Triple Product Wavelet Integrals for All-Frequency Relighting. *ACM Trans. Graph. 23,* 3, 477–487.

Nielson, G. M., Jung, I.-H., and Sung, J. 1997. Haar Wavelets over Triangular Domains with Applications to Multiresolution Models for Flow over a Sphere. In *VIS '97: Proceedings of the 8th Conference on Visualization '97*. IEEE Computer Society Press, Los Alamitos, CA, USA, 143–ff.

Pratt, W. K. 1991. *Digital Image Processing (2nd ed.)*. John Wiley & Sons, Inc., New York, NY, USA.

Ramamoorthi, R. and Hanrahan, P. 2002. Frequency Space Environment Map Rendering. In *SIGGRAPH '02: ACM SIGGRAPH 2002 Papers*. ACM Press, New York, NY, USA, 517–526.

Roşca, D. 2005. Haar Wavelets on Spherical Triangulations. In *Advances in Multiresolution for Geometric Modelling*, N. A. Dodgson, M. S. Floater, and M. A. Sabin, Eds. Mathematics and Visualization. Springer Berlin Heidelberg, 405–417.

Schröder, P. and Sweldens, W. 1995. Spherical Wavelets: Efficiently Representing Functions on the Sphere. In *SIGGRAPH '95: Proceedings of the 22nd annual Conference on Computer Graphics and Interactive Techniques*. ACM Press, New York, NY, USA, 161–172.

Sillion, F., Arvo, J., Westin, S., and Greenberg, D. P. 1991. A Global Illumination Solution for General Reflectance Distributions. In *SIGGRAPH '91: Proceedings of the 18th Annual Conference on Computer Graphics and Interactive Techniques*. ACM Press, New York, NY, USA, 187–196.

Sloan, P.-P., Kautz, J., and Snyder, J. 2002. Precomputed Radiance Transfer for Real-Time Rendering in Dynamic, Low-Frequency Lighting Environments. In *SIGGRAPH '02: ACM SIGGRAPH 2002 Papers*. ACM Press, New York, NY, USA, 527–536.

Sloan, P.-P., Luna, B., and Snyder, J. 2005. Local, Deformable Precomputed Radiance Transfer. In *SIGGRAPH '05: ACM SIGGRAPH 2005 Papers*. ACM Press, New York, NY, USA, 1216–1224.

Stollnitz, E. J., Derose, T. D., and Salesin, D. H. 1996. *Wavelets for Computer Graphics: Theory and Applications*. Morgan Kaufmann Publishers Inc., San Francisco, CA, USA.

Sun, W. and Mukherjee, A. 2006. Generalized Wavelet Product Integral for Rendering Dynamic Glossy Objects. *ACM Trans. Graph. 25,* 3, 955–966.

Sweldens, W. 1996. The Lifting Scheme: A Custom-Design Construction of Biorthogonal Wavelets. *Appl. Comput. Harmon. Anal. 3,* 2, 186–200.

Todhunter, I. 1901. *Spherical Trigonometry, for the Use of Colleges and Schools*. Macmillan, London.

Tsai, Y.-T. and Shih, Z.-C. 2006. All-Frequency Precomputed Radiance Transfer using Spherical Radial Basis Functions and Clustered Tensor Approximation. In *SIGGRAPH '06: ACM SIGGRAPH 2006 Papers*. ACM Press, New York, NY, USA, 967–976.

Wang, R., Ng, R., Luebke, D., and Humphreys, G. 2006. Efficient Wavelet Rotation for Environment Map Rendering. In *Proceedings of the 2006 Eurographics Symposium on Rendering*. Springer-Verlag, Vienna. Published as Rendering Techniques 2006.

Westin, S. H., Arvo, J. R., and Torrance, K. E. 1992. Predicting Reflectance Functions from Complex Surfaces. In *SIGGRAPH '95: ACM SIGGRAPH 1992 Papers*. ACM Press, New York, NY, USA, 255–264.

Zhou, K., Hu, Y., Lin, S., Guo, B., and Shum, H.-Y. 2005. Precomputed Shadow Fields for Dynamic Scenes. In *SIGGRAPH '05: ACM SIGGRAPH 2005 Papers*. ACM Press, New York, NY, USA, 1196–1201.

Received May 2007, revised May 2007, accepted May 2007

A. APPENDIX

Derivation of the wavelet basis functions for the SOHO wavelet basis (Mathematica document): http://www.dgp.toronto.edu/ lessig/soho/data/solution_wavelets.nb

B. APPENDIX

Development of a spherical subdivision scheme with area-isometry for the three outer child triangles (Mathematica document):
http://www.dgp.toronto.edu/ lessig/soho/data/solution_area_equality.nb